Scientific Research Publishing

Advances in Materials Physics and Chemistry, 2026, 16(6), 234-248
https://www.scirp.org/journal/ampc
ISSN Online: 2162-5328
ISSN Print: 2162-531X

Communication: Phase Diagram, Microstructure and Atomistic 2nd Law of Thermodynamics

Kuochung Liu*

Independent Researcher, Kaohsiung
Email: *kcliu05915@gmail.com

How to cite this paper: Liu, K.C. (2026) Communication: Phase Diagram, Microstructure and Atomistic 2nd Law of Thermodynamics. *Advances in Materials Physics and Chemistry*, **16**, 234-248.
https://doi.org/10.4236/ampc.2026.166012

Received: April 28, 2026
Accepted: June 2, 2026
Published: June 5, 2026

Abstract

The Atomistic 2nd Law of Thermodynamics and its necessary and sufficient condition can be used to explain the phase diagrams of one or two components. In these explanations, the lowest molar total chemical potential of atomistic features plays an important role, while the common tangent and lever rule are useful in understanding binary phase diagrams. In explaining the microstructural evolution at a composition of a binary phase diagram, the driving force, the mobility of atomistic features and lever rule etc. can be well applied. Recently the use of machines or AI in the optimization of material properties is highly valued. More effective results could be obtained if the users of these tools have better understanding of the Atomistic 2nd Law of Thermodynamics and kinetics. The discussed topics are: T-T-T curves and phase diagrams, T-T-T curves of 1080 steel, T-T-T curves of other materials, systems containing low-melting impurities.

Keywords

Phase Diagram, Atomistic 2nd Law, Chemical Potential, Microstructure, Property, AI, T-T-T Curve, Driving Force, Mobility, Slags

1. Introduction

The Atomistic 2nd Law of Thermodynamics can be regarded as the widening of the Classic 2nd Law of Thermodynamics which was developed in 19th to early 20th centuries when atomistic views were not yet popular. The latter is very useful to spontaneous equilibrium systems when contents, temperatures and/or pressures are controllable, such as engineering problems. While the former can be applied widely to spontaneous equilibrium systems with various driving forces, including

chemical potentials, gravitational potential, electrical potential, magnetic potential etc. (e.g. capillary phenomena are due to the combined driving forces of chemical potential and gravitational potential). For the one-component equilibrium system where chemical potential is the only important potential, a comparison between Classic 2nd Law of Thermodynamics and Atomistic 2nd Law of Thermodynamics was made in the Table 1[1] of reference [1].

In references [1], the theory and applications of Atomistic 2nd Law of Thermodynamics were described in detail. In references [2], some elucidating phenomena of Atomistic 2nd Law of Thermodynamics were followed. References [1] proposed that: the chemical potential of condensed phases originated from the bonding potential of atomistic features[2], whereas the chemical potential of a gas phase originated from the concentration of its atomistic features. These papers also proposed that, the driving force for spontaneous equilibrium in the system came from the Atomistic 2nd Law of Thermodynamics which was: the molar total potential[3] of atomistic features would evolve toward the lowest value.

The necessary and sufficient condition of this rule was: the molar total potential was equal everywhere in the system. When the potentials other than chemical potential can all be neglected, "molar total potential" becomes "molar total chemical potential[4]". When there are extra driving forces in the system (e.g. mechanical stirring, differential ΔP in reverse osmosis or blood pressure ΔP), it's necessary to consider these extra driving forces together with the spontaneous driving forces.

Phase diagrams are to display the equilibrium phases in a system under various conditions such as temperature, pressure and composition. Equilibrium can be achieved via two ways. One way is: the molar total chemical potential of atomic species is at the lowest value (*i.e.* the Atomistic 2nd Law of Thermodynamics itself); the second way is: equilibrium phases have the same molar total chemical potential (*i.e.* the necessary and sufficient condition of the Atomistic 2nd Law of Thermodynamics).

In one-component phase diagrams, single-phase zones show the stable phases which have the lowest chemical potentials at various pressures and temperatures; while the boundaries show the neighboring phases have equal chemical potentials at the indicated temperatures and pressures. Hence one-component phase diagrams have a close relation to the Atomistic 2nd Law of Thermodynamics.

A typical binary phase diagram includes the following: 1) Single phase zones: at various temperature, the molar total chemical potential of the system is lowered

[1]In this Table, the total chemical potential (*i.e.* N·μ) is the only parameter used in the Atomistic 2nd Law of Thermodynamics when temperatures and/or pressures are changed in the system. Whereas the Classic 2nd Law of Thermodynamics needs different parameters for different conditions such as S, E, H, F and G. Hence it's not hard to see that the Atomistic 2nd Law of Thermodynamics is simpler.

[2]As defined in references [1], the atomistic features include atoms, molecules, ions, electrons and etc.

[3]Molar total potential is defined as "the overall potential that one mole of atomistic features possess" due to the interactions among atomistic features (*i.e.* chemical potentials) as well as the potentials arising from the interactions between atomistic features and the environment, e.g. gravitational potential, electric potential, magnetic potential and etc.

[4]Molar total chemical potential is defined as the total potential that one mole of atomistic features possess due to the interactions among atomistic features.

due to the dissolution of one component into the other (until saturation); 2) Co-existing zones of two phases: the molar total chemical potential is the lowest for co-existing phases at certain ratio (lever rule is applicable) at each co-existing composition and temperature; 3) Eutectic (or Eutectoid) point: the molar total chemical potential is the lowest at this specified composition and temperature. 4) Boundaries: at indicated compositions and temperatures, the neighboring phases have equal molar total chemical potential. Hence binary phase diagrams also have a close relation to the Atomistic 2nd Law of Thermodynamics.

Some documents showed binary phase diagrams together with the evolution of microstructures at certain composition. Although these figures are helpful to understand the relation between microstructures and phase diagrams, an in-depth explanation is mostly not offered. The author believes, phase diagrams and their near equilibrium microstructures (stable single crystals are without grain boundaries and are truly at equilibrium) can be well explained via the Atomistic 2nd Law of Thermodynamics, its necessary and sufficient condition as well as kinetics. The following are some studies related to these topics.

2. Phase Diagrams and the Atomistic 2nd Law of Thermodynamics

The analyses in this section are mostly for binary phase diagrams, while the descriptions for one-component or three-component on phase diagrams are only brief.

2.1. One Component

For the phase diagrams of one-component, normally the X-axis is temperature and the Y-axis is pressure. Figure 1 is the phase diagram for water [3]:

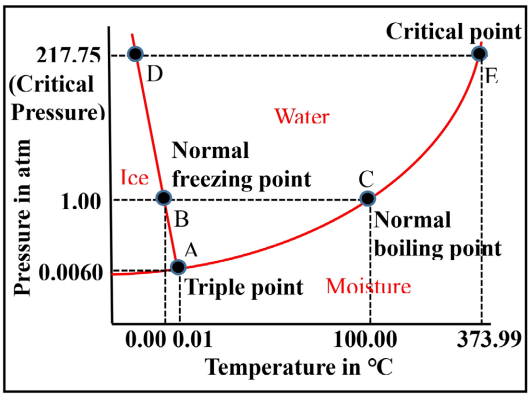

Figure 1. Phase diagram for water.

In Figure 1, the single phase zones of ice, water and moisture show that these phases have the lowest molar chemical potential for water molecules at the indicated temperature and pressure. Figure 1 also shows two red curves separating ice, water and moisture. The phases on the two sides of red curves are at equilib-

rium at the temperatures and pressures indicated, because both phases have the same molar chemical potential. For example, ice and water are at equilibrium at 1atm and 0˚C (point B), and water and moisture are at equilibrium at 1atm and 100˚C (point C); while all 3 phases are at equilibrium at 0.0060 atm and 0.01˚C (triple point A). Figure 1 also shows: when the pressure is less than 1 atm (e.g. at mountains), water will boil at a temperature less than 100˚C.

Another example is in the phase diagram of carbon. It is known that at room temperature and pressure the stable phase is graphite, and diamond is metastable (like a glass). Due to kinetic constraints, a diamond is unable transforming to graphite thus can be kept forever at room temperature and pressure (also like a glass). According to the phase diagram of carbon [4], diamond is the stable phase of carbon at very high pressure.

2.2. Two-Component A and B

When B dissolves in A as α phase, according to the Atomistic 2nd Law of Thermodynamics, the molar total chemical potential of α phase at composition X (denoted as μ_α (X)) will decrease from μ_α (0) until saturated at X_α. When $X > X_\alpha$, μ_α (X) increases again. Hence, μ_α (X) is a concave upward curve with composition X. Similarly, μ_L (X) of liquid phase and μ_β (X) of β phase are also concave upward curves with composition X, as shown in **Figure 2**.

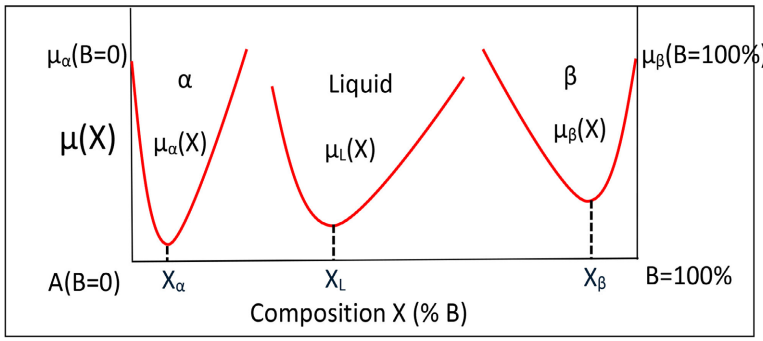

Figure 2. The μ (X) of α, β and L phases are all concave upward curves.

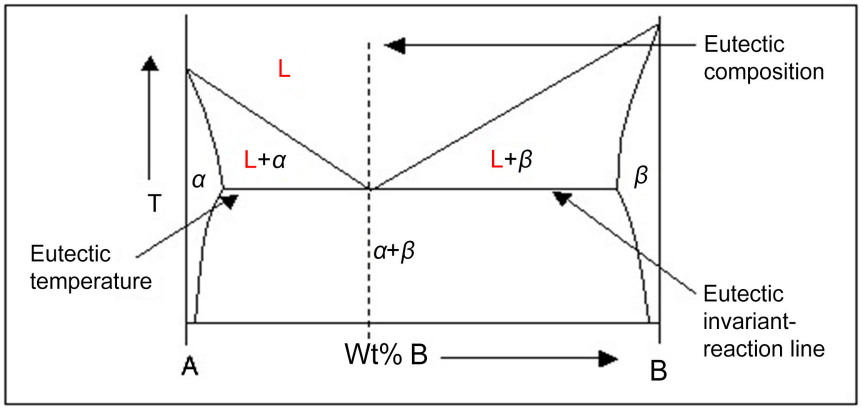

Figure 3. A typical binary phase diagram with components A and B.

In a typical binary phase diagram, X-axis is composition, Y-axis is temperature and pressure is kept at 1atm. Figure 3 [5] is a binary phase diagram with components A and B. In Figure 3, there are several single phase zones (*i.e.* liquid L, α phase, β phase), an Eutectic composition, an Eutectic temperature, several co-existing zones as well as boundaries (although peritectic and **peritectoid** reactions are not studied, the author believes the rules are the same).

2.2.1. At Eutectic Temperature

According to the Atomistic 2nd Law of Thermodynamics, at Eutectic temperature the molar total chemical potential of composition X (denoted by $\mu(X)$) is the lowest. It is known from Figure 3, $\mu(X)$ comes from α phase, Liquid + α phase, Liquid + β phase and β phase when X increases. Hence $\mu(X)$ can be shown as the red curve of Figure 4 (E denotes Eutectic point, X_{LE} denotes Eutectic composition):

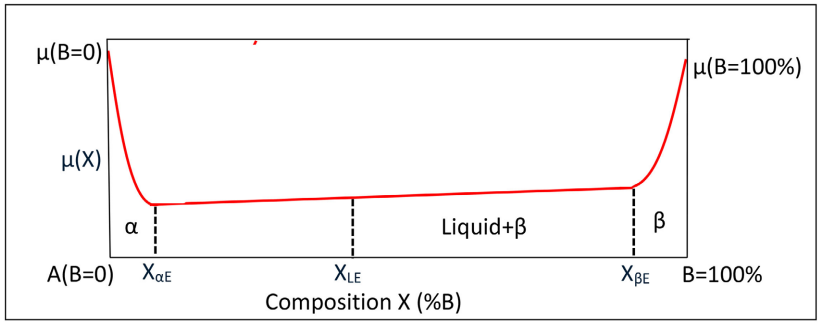

Figure 4. The red curve is the lowest $\mu(X)$ between A and B at Eutectic temperature.

I.e. $\mu(X)$ is as follows:

$$\begin{aligned}&\text{When } 0 \le X \le X_{\alpha E}, \mu(X) = \mu_\alpha(X),\\ &\text{When } X_{\alpha E} \le X \le X_{\beta E}, \mu(X) = \mu_\alpha(X_{\alpha E})\\ &\qquad + \left\{\left[\mu_\beta(X_{\beta E}) - \mu_\alpha(X_{\alpha E})\right] \div (X_{\beta E} - X_{\alpha E})\right\} \cdot (X - X_{\alpha E}),\\ &\text{When } X_{\beta E} \le X \le 100\%, \mu(X) = \mu_\beta(X)\end{aligned} \quad (1)$$

The characteristics of (Equation 1) include:

a) $[\mu_\beta(X_{\beta E}) - \mu_\alpha(X_{\alpha E})] \div (X_{\beta E} - X_{\alpha E})$ is the slope of the common tangent in Liquid + α zone as well as in Liquid+β zone. In this equation $\mu_\beta(X_{\beta E})$, $\mu_\alpha(X_{\alpha E})$, $X_{\beta E}$, and $X_{\alpha E}$ are all constants.

b) Lever rule can be applied to the co-existing zones: for example when $X_{\alpha E} \le X \le X_{LE}$, the ratio of Liquid phase is $(X - X_{\alpha E}) \div (X_{LE} - X_{\alpha E})$. Similarly when $X_{LE} \le X \le X_{\beta E}$, the ratio of β phase is $(X - X_{LE}) \div (X_{\beta E} - X_{LE})$.

2.2.2. At Temperatures Slightly Higher than Eutectic Temperature

At this temperature, liquid is in a single phase zone. Similar to at Eutectic temperature, Figure 3 shows that the lowest $\mu(X)$ between A and B comes from $\alpha 1$ phase, Liquid + $\alpha 1$ zone, Liquid phase, Liquid + $\beta 1$ zone and $\beta 1$ phase when X increases, as shown in the red curve of Figure 5:

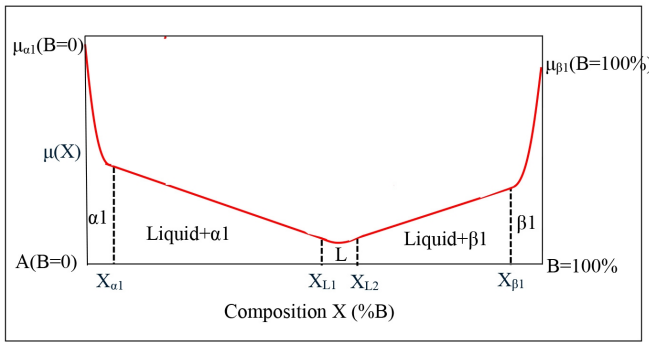

Figure 5. The red curve is the lowest μ (X) between A and B at Slightly Higher than Eutectic Temperature.

I.e. μ (X) is as follows:

$$\begin{aligned}
&\text{When } 0 \leqq X \leqq X_{\alpha 1}, \mu(X) = \mu_{\alpha 1}(X),\\
&\text{When } X_{\alpha 1} \le X \le X_{L1}, \mu(X) = \mu_{\alpha 1}(X_{\alpha 1}) + \left\{\left[\mu_L(X_{L1}) - \mu_{\alpha 1}(X_{\alpha 1})\right] \div (X_{L1} - X_{\alpha 1})\right\} \cdot (X - X_{\alpha 1}),\\
&\text{When } X_{L1} \le X \le X_{L2}, \mu(X) = \mu_L(X),\\
&\text{When } X_{L2} \le X \le X_{\beta 1}, \mu(X) = \mu_L(X_{L2}) + \left\{\left[\mu_{\beta 1}(X_{\beta 1}) - \mu_L(X_{L2})\right] \div (X_{\beta 1} - X_{L2})\right\} \cdot (X - X_{L2}),\\
&\text{When } X_{\beta 1} \le X \le 100\%, \mu(X) = \mu_{\beta 1}(X)
\end{aligned} \tag{2}$$

The characteristics of (Equation 2) include:

a) $[\mu_L(X_{L1}) - \mu_{\alpha 1}(X_{\alpha 1})] \div (X_{L1} - X_{\alpha 1})$ is the slope of the common tangent in Liquid + $\alpha 1$ zone; while $[\mu_{\beta 1}(X_{\beta 1}) - \mu_L(X_{L2})] \div (X_{\beta 1} - X_{L2})$ is the slope of the common tangent in Liquid+$\beta 1$ zone.

b) Lever rule can be applied: when $X_{\alpha 1} \le X \le X_{L1}$, the ratio of Liquid phase is $(X - X_{\alpha 1}) \div (X_{L1} - X_{\alpha 1})$. Similarly, when $X_{L1} \le X \le X_{\beta 1}$, the ratio of $\beta 1$ phase is $(X - X_{L1}) \div (X_{\beta 1} - X_{L1})$.

c) In **Figure 3** when the temperature rises from Eutectic temperature, since the boundaries of Liquid + $\alpha 1$ zone and Liquid + $\beta 1$ zone are not vertical, $X_{\alpha 1} \neq X_{\alpha E}$, $X_{\beta 1} \neq X_{\beta E}$, and phase $\alpha 1 \neq$ phase α, phase $\beta 1 \neq$ phase β.

2.2.3. At Temperatures Slightly Lower than Eutectic Temperature

In this case **Figure 3** shows the equilibrium phases are only $\alpha 2$ phase, $\alpha 2 + \beta 2$ zone and $\beta 2$ phase. Similarly, between A and B the lowest μ (X) is from $\alpha 2$ phase, $\alpha 2 + \beta 2$ zone and $\beta 2$ phase when X increases, as shown in **Figure 6**.

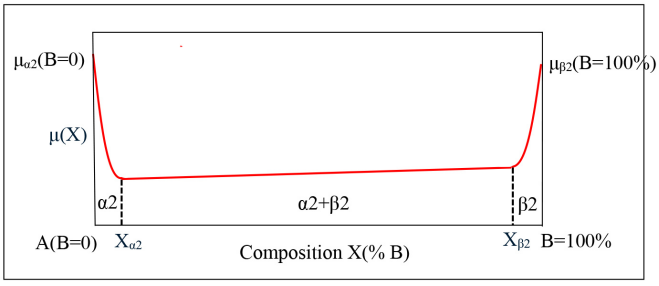

Figure 6. The red curve is the lowest μ (X) between A and B at Slightly Lower than Eutectic Temperature.

I.e. $\mu(X)$ is as follows:

$$\begin{aligned}&\text{When } 0 \le X \le X_{\alpha 2}, \mu(X) = \mu_{\alpha 2}(X)\\ &\text{When } X_{\alpha 2} \le X \le X_{\beta 2}, \mu(X) = \mu_{\alpha 2}(X_{\alpha 2}) + \left\{\left[\mu_{\beta 2}(X_{\beta 2}) - \mu_{\alpha 2}(X_{\alpha 2})\right] \div (X_{\beta 2} - X_{\alpha 2})\right\} \cdot (X - X_{\alpha 2}) \quad (3)\\ &\text{When } X_{\beta 2} \le X \le 100\%, \mu(X) = \mu_{\beta 2}(X)\end{aligned}$$

The characteristics of (Equation 3) include:

a) $[\mu_{\beta 2}(X_{\beta 2}) - \mu_{\alpha 2}(X_{\alpha 2})] \div (X_{\beta 2} - X_{\alpha 2})$ is the slope of the common tangent in $\alpha 2 + \beta 2$ zone.

b) Lever rule can be applied to $\alpha 2 + \beta 2$ zone: when $X_{\alpha 2} \le X \le X_{\beta 2}$, the ratio of phase $\beta 2$ is $(X - X_{\alpha 2}) \div (X_{\beta 2} - X_{\alpha 2})$.

c) In Figure 3 when the temperature is slightly lower than Eutectic temperature, since the boundaries of $\alpha 2 + \beta 2$ zone are not vertical, $X_{\alpha 2} \ne X_{\alpha E}$, $X_{\beta 2} \ne X_{\beta E}$ and phase $\alpha 2 \ne$ phase $\alpha 1$, phase $\beta 2 \ne$ phase $\beta 1$.

2.3. Three-Component

When there are three components in a system, the phase diagrams become quite complicated although the basic rules are the same. In this condition, normally temperature and pressure are fixed, and each side of a triangle is used for the compositions of each component. Reference [6] has detailed explanations for ternary phase diagrams.

In Co-Ti-Ta system, Wang *et al.* [7] displayed three binary phase diagrams to show the relations among components. Electron probe micro-analyzer and X-ray diffraction were used as tools for their experimental verifications.

3. Microstructure and Phase Diagram

3.1. Evolution of Microstructure in Pb-Sn Alloy

When the microstructural evolution at one composition is shown together with a binary phase diagram, it's convenient to study the relation between them. Figure 7 is an example showing the phase diagram of Pb-Sn alloy and the microstructural evolution at composition C_4 [8].

In Figure 7, the microstructures at composition C_4 have the following characteristics:

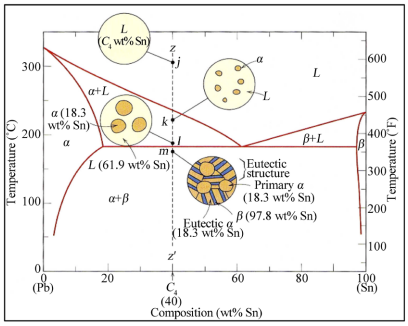

Figure 7. Phase diagram of Pb-Sn alloy and the microstructural Evolution at composition C_4 (L denotes liquid).

3.1.1. α + L Zone

a) When the temperature is lowered from liquid zone to α + L zone, there is a driving force to precipitate α crystals from liquid. In this case, α crystals are convex and close to spherical (to lower the molar total chemical potential due to the surface of α crystals).

b) When the temperature is further lowered and the system is further away from liquid zone, the driving force to precipitate α crystals will increase. But the mobility of atomistic species is lower which is unfavorable to nucleation. Possibly due to this reason the density of α crystals at point l is apparently lower than that at point k.

c) The composition of α crystals at point l is ~18.3 wt% Sn, whereas the composition of liquid at point l is ~61.9 wt% Sn. According to lever rule: the ratio of α crystal at point l is higher than that of point k. All these results comply with the phase diagram shown in **Figure 7**.

3.1.2. α + β Zone

a) In this case, the main driving force for phase transition is to precipitate solid α and solid β crystals simultaneously from the rest liquid. The α crystals already appeared at point l remain at point m.

b) The microstructure at point m shows: the α and β crystals transformed from liquid are with alternating lamellar structure. The newly formed α crystals at point m apparently have a different shape from the α crystals already formed at point l. This lamellar structure might be related to kinetics, e.g. diffusion of atomistic species (as also discussed in [8]).

c) The α crystals in alternating lamellar structure contain ~18.3 wt% Sn, while the β crystals contain ~97.8 wt% Sn, both complying with **Figure 7**.

d) When cooled from the Eutectic composition, since the solid α crystals and solid β crystals precipitate simultaneously with very different compositions, it's not surprising to see that α crystals and β crystals appear with alternating lamellar structure (or rod-like), as reported in many studies (including [8]).

3.2. Evolution of Microstructure in a Carbon Steel

Figure 8 is a part of the phase diagram of a carbon steel and the microstructural evolutions at composition C_0 [9].

The characteristics of **Figure 8** include:

a) The phase transition from point c to point d is to precipitate α crystals from the grain boundary of γ crystals where the molar total chemical potential is higher (because of less complete bonding). These α crystals are close to spherical to reduce the molar total chemical potential of α crystals.

b) The Proeutectoid α crystals at point e are not only larger, but also apparently deviate from being spherical. A logical reasoning is: the growth of Proeutectoid α crystals is along the boundaries of solid γ crystals where the molar total chemical potentials are higher, therefore are not near spherical any more.

Similar to Figure 7, the density of Proeutectoid α crystals at point e of Figure 8 is slightly lower than that at point d, while the ratio of Proeutectoid α crystal at point e is higher than that at point d, complying with lever rule.

c) Similar to 3.1.2 (b), the Eutectoid α crystals simultaneously appearing with Fe_3C are with alternating lamellar structure.

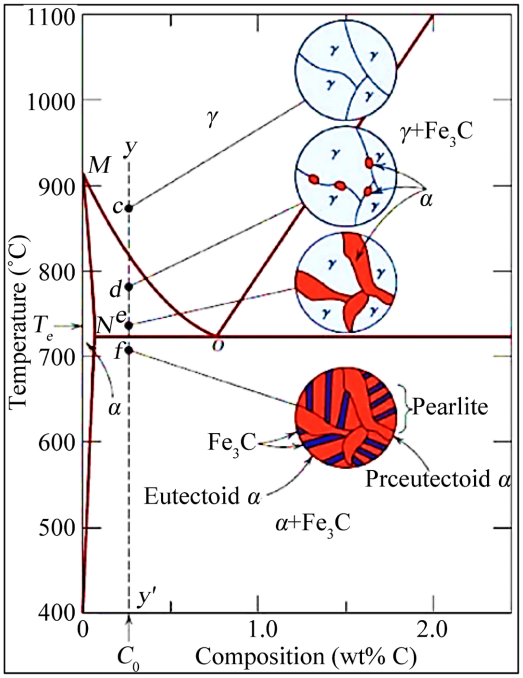

Figure 8. Part of iron carbon phase diagram and the evolution of microstructures at C_0 (γ crystals is austenite).

3.3. Improvement of Properties via Microstructure

The microstructure of materials can be totally at equilibrium (a stable single crystal), nearly at equilibrium (poly-crystal), totally non-equilibrium (quenched materials) or somewhere among them, and can have a morphology controlled by various mechanisms (e.g. cooling rate control, diffusion control and etc.). Therefore, the microstructural modification for better properties is a huge area. Some related researches are as follows:

a) Kathavate *et al.* [10] used additives in multilayered complex structures to improve their microstructures so that superior mechanical, thermal, chemical and physical properties can be obtained.

b) Wang *et al.* [11] investigated the relation among the microstructure of a titanium alloy, fracture toughness and crack propagation, and find a better combination of strength, ductility and fracture toughness.

c) The stability and lifetime of devices are related to the microstructures of materials, thus modifying microstructures is a means to improve the performance of devices. For example, Wong *et al.* [12] used diffusion-controlled morphology modification to improve the stability of organic photovoltaics.

3.4. Use of Machine or AI in Designing Materials

In recent years, the use of machine or AI (artificial intelligence) as a tool to improve the microstructures and properties of materials is much valued. The following are related studies:

a) Whitman *et al.* [13] published a paper stressing on the rise of computational materials science. The methods were based on the microstructure-property relationships from data. In addition, two case studies were demonstrated.

b) Madika *et al.* [14] published a review paper on the recent impact of artificial intelligence (AI), machine learning (ML), and deep learning (DL) on materials science, emphasizing on materials discovery, development and optimization.

The author believes, if the users of these tools have better understanding of the Atomistic 2nd Law of Thermodynamics and of kinetics, their work would be more effective and better results could be obtained.

4. Discussion

4.1. T-T-T Curves and Phase Diagrams

In a typical T-T-T curve, the Y-axis is temperature and the X-axis is time. The 1st solid line shows "the time needed for the initiation of phase transition at various temperatures". The 2nd solid line shows "the time needed for 100% of phase transition at various temperatures". It is not hard to see that T-T-T curves are very different from phase diagrams in nature.

However, the driving force for both T-T-T curves and phase diagrams is "the lowering of molar total chemical potential of atomistic features", it's only natural that they have the same phase transitions. The following analyses of T-T-T curves are based on Atomistic 2nd Law of thermodynamics and kinetics.

4.2. T-T-T Curves for 1080 Steel

The T-T-T curves for 1080 steel is shown in **Figure 9** [15]. These T-T-T curves have a typical C-shape and can be used as an example to elaborate on the characteristics of T-T-T curves:

a) The upper part of a T-T-T curve: Whether for 0%, 50% or 100%, the time needed for phase transitions are gradually prolonged as Eutectoid temperature (727˚C) is approached, and phase transitions all stop at Eutectoid temperature. This phenomenon shows: the time needed for phase transition is inversely related to the driving force of atomic specie. When the temperature is very close to Eutectoid temperature, the driving force of atomic species is ~0 and the time needed for phase transition is ~∞, even though the mobility of atomic species is higher at higher temperature.

b) The noses of T-T-T curves: Whether for 0%, 50% or 100% phase transition, the shortest time appears at certain middle temperature (lower than Eutectoid temperature), although the driving force for phase transitions is not the largest (smaller than lower temperatures). Hence, T-T-T curves have noses at cer-

tain middle temperature, showing the largest combined effect of driving force and mobility. Moreover, the nose of the first curve appears after a short time (not at zero time). A logical explanation is: the phase transition of atomic species has to overcome the activation energy for phase transition, and needs time to gather and nucleate.

c) The lower part of a T-T-T curve: Whether for 0%, 50% or 100% phase transition, although the decrease of temperature means further away from Eutectoid temperature and a higher driving force for phase transition, but the time needed for phase transition is gradually prolonged. This phenomenon shows: the driving force of atomic species is not as important as their mobility; hence the time needed for phase transition is longer when the mobility is lower.

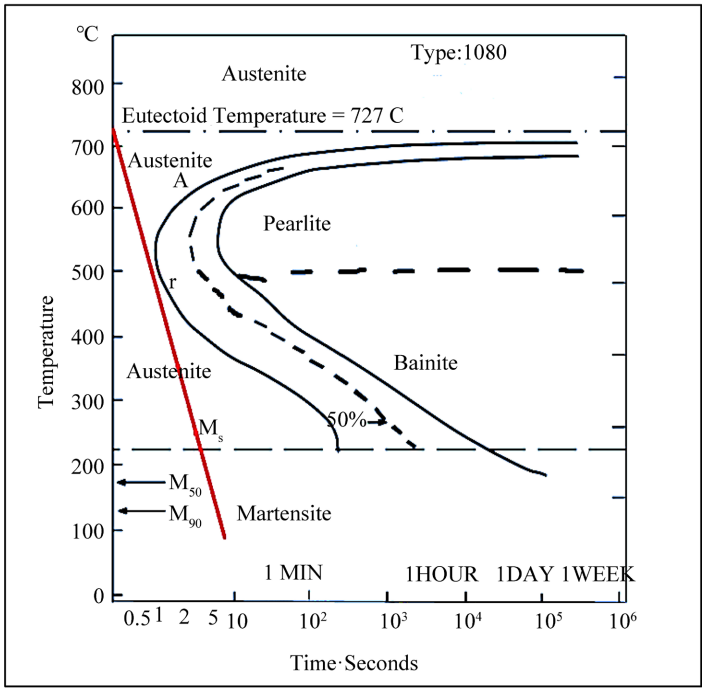

Figure 9. T-T-T curves for 1080 steel.

The red line in **Figure 9** does not touch the T-T-T curves of Pearlite or Bainite for 1080 steel, hence only Martensite is formed after cooling. This Martensitic steel can be tempered to obtain the needed crystals. Conversely, if the cooling of 1080 steel crosses the T-T-T curves of these crystals, the corresponding crystals will be formed.

4.3. T-T-T Curves for Other Materials

T-T-T curves are often used for steels. Since the basic rules (*i.e.* the Atomistic 2nd of Thermodynamics and kinetics) are the same for other materials, similar T-T-T curves can be established and used. For example, Onike *et al.* [16] established the T-T-T curves for Kaolinite in 1986, Liu *et al.* [17] established T-T-T curves for the reaction sintering between Kaolinite and Alumina in 1994; Long *et al.* [18] used a

T-T-T curve in the glass-forming ability of a metal alloy in 2009; Martín *et al.* [19] used the T-T-T curves to depict the crystallization behavior of a glass fiber in 2014.

4.4. Systems Containing Low-Melting Impurities

Figure 10 [20] is a picture of DDF (Darkfield Diffraction) in TEM (Transmission Electron Microscopy), showing the mullite crystals are surrounded by a glassy thin film and glassy pockets. This glassy phase comes from the low-melting impurities of raw materials.

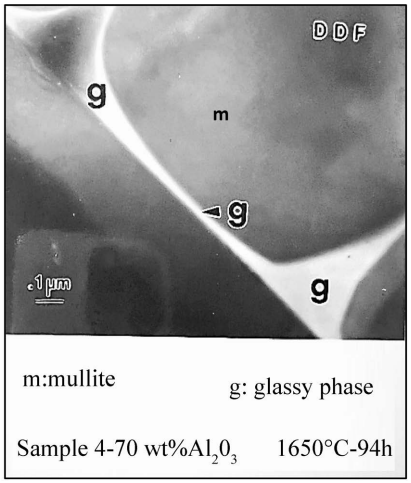

Figure 10. A TEM picture showing the mullite crystals (m) are surrounded by a glassy thin film and glassy pockets (g).

Ceramic raw materials normally contain low-melting impurities that will form liquid at low temperatures. When the cooling of the system is fast enough, this liquid does not touch the T-T-T curves of its crystals, thus a co-existing glassy phase is formed. For example, there are small amounts of low-melting impurities in Kaolinite and Alumina materials, including K_2O (melting point~700˚C), Na_2O (melting point~1132˚C) or FeO (melting point < 1400˚C). When the mixture of Kaolinite and Alumina was reaction sintered at 1650˚C to form mullite, a co-existing glassy phase would appear after furnace cooling.

The mechanical property of impurity-containing glassy phase should not be important. Metallurgical slags contain many low-melting impurities and is easy to become glassy phase. Shang *et al.* [21] systematically reviewed the advances in utilizing metallurgical slags to manufacture glass ceramics. Their special attention was devoted to the challenges from the aspects of cost, safety and diversification in preparing the glass-ceramics from metallurgical slags and to corresponding solutions for maximizing utilization of the wastes with desirable product quality.

Du *et al.* [22] used heavy metal containing blast furnace slag in the manufacture of high performance glass ceramics. They observed that the leaching concentrations of Zn, Mn, Cr in products were much lower than the standard values of hazardous waste leaching toxicity. These results indicated that glass ceramics also

have good curing effects.

5. Conclusions

1) The rule of the Atomistic 2nd Law of Thermodynamics for spontaneous equilibrium is: the molar total chemical potential in the system is the lowest. Its necessary and sufficient condition is: the co-existing phases at equilibrium have the same molar total chemical potential. These rules can be applied to the phase diagrams of single component (e.g. water or carbon) as well as to binary phase diagrams. The elaborated examples of these rules in binary phase diagrams are: at Eutectic temperature, slightly higher than Eutectic temperature and slightly lower than Eutectic temperature. The common tangent and lever rule are also used in binary examples.
2) In literature, the phase diagram of Pb-Sn alloy was displayed together with the microstructural evolution at a composition. The phase diagram of a carbon steel was also displayed together with the microstructural evolution at a composition. It is known from this phase diagram that the microstructures of precipitated crystals can be close to spherical or far away from spherical, can be with different sizes, with different densities, and with alternating lamellar structure. The author explains these phenomena rationally based on the Atomistic 2nd Law of Thermodynamics and kinetics.
3) The microstructure of a material can be totally at equilibrium (a stable single crystal), close to equilibrium (poly-crystal), or very far away from equilibrium (quenched materials), or somewhere among them, and can have a morphology controlled by various mechanisms. Therefore, the range of microstructures is very wide. In recent years, the use of machine or AI for superior material properties is highly valued. The author believes, these tools should be more effective if the users are with a better understanding of the Atomistic 2nd Law of Thermodynamics and of kinetics.
4) A T-T-T curve shows the time needed in a system for certain degree of phase transition under various temperatures. Hence, the dynamic nature of T-T-T curves is different from phase diagrams. From the viewpoints of driving force and mobility of atomistic species, the author explains the formation of a T-T-T curve in detail. The small amount of time needed to initiate the T-T-T curves is explained rationally via activation energy and nucleation. Although T-T-T curves are often used in steel, the rules involved are also applicable to other materials.
5) The raw materials for ceramics normally contain low-melting impurities, hence liquid will appear at low temperatures. During cooling, this co-existing and enclosing liquid will form a glassy phase, because it does not touch the T-T-T curves of its crystalline phase (s). It was reported that some heavy-metals containing metallurgical slags can be used as the raw materials for high performance glass ceramics. The leaching concentrations of Zn, Mn, and Cr ions in products were much lower than the standards for hazardous waste leaching

toxicity. Therefore, metallurgical slags can be reused for this value-added purpose without environmental concerns.

Conflicts of Interest

The author declares no conflicts of interest regarding the publication of this paper.

References

[1] Liu, K. (2025) Communication: A Simpler and More Applicable 2nd Law of Thermodynamics. *Advances in Materials Physics and Chemistry*, **15**, 39-59. https://doi.org/10.4236/ampc.2025.153003

[2] Liu, K. (2025) Communication: Phenomena That Could Make the Atomistic 2nd Law of Thermodynamics Clearer. *Advances in Materials Physics and Chemistry*, **15**, 101-116. https://doi.org/10.4236/ampc.2025.157007

[3] Phase Diagram for Water. https://courses.lumenlearning.com/umes-cheminter/chapter/phase-diagram-for-water/

[4] Wikipedia (2026) Carbon. https://en.wikipedia.org/wiki/Carbon

[5] Phase Diagrams 2-Eeutectic Reactions. https://www.doitpoms.ac.uk/tlplib/phase-diagrams/phasediags2.php

[6] Lee, S. (2025) Ternary Phase Diagrams: Theory and Practice: A Detailed Exploration for Researchers and Practitioners。 https://www.numberanalytics.com/blog/ternary-phase-diagrams-theory-practice

[7] Wang, C., Zhang, X., Li, L., Pan, Y., Chen, Y., Yang, S., *et al.* (2018) Phase Equilibria of the Co-Ti-Ta Ternary System. *Metals*, **8**, Article 958. https://doi.org/10.3390/met8110958

[8] A Practical Guide to Phase Diagrams. https://phasediagram.weebly.com/eutectics.html

[9] Tsenenko, D. (2019) EXATIN INFORM. https://exatin.info/iron-carbon-phase-diagram/

[10] Kathavate, V.S. and Eswar Prasad, K. (2025) Microstructure Evolution and Mechanical Properties of Alloys Fabricated via Additive Manufacturing. In: Rathee, S., Srivastava, M. and Paulo Davim, J., (Eds.), *Metal Additive Manufacturing*, Springer, 131-162. https://doi.org/10.1007/978-981-96-8162-4_8

[11] Wang, H., Zhao, Q., Xin, S., Zhao, Y., Zhou, W. and Zeng, W. (2021) Microstructural Morphology Effects on Fracture Toughness and Crack Growth Behaviors in a High Strength Titanium Alloy. *Materials Science and Engineering*: *A*, **821**, Article ID: 141626. https://doi.org/10.1016/j.msea.2021.141626

[12] Wang, Y., Gao, H., Sun, M., Lin, C., Li, H., Lin, F.R., *et al.* (2024) Diffusion-Controlled Morphology Modification via Employing Host/Guest Acceptors to Improve the Stability of Organic Photovoltaics. *Advanced Energy Materials*, **14**, Article ID: 2304449. https://doi.org/10.1002/aenm.202304449

[13] Whitman, S.E. and Latypov, M.I. (2025) Machine Learning of Microstructure-Property Relationships in Materials Leveraging Microstructure Representation from Foundational Vision Transformers. *Acta Materialia*, **296**, Article ID: 121217. https://doi.org/10.1016/j.actamat.2025.121217

[14] Madika, B., Saha, A., Kang, C., Buyantogtokh, B., Agar, J., Wolverton, C.M., *et al.* (2025) Artificial Intelligence for Materials Discovery, Development, and Optimiza-

tion. *ACS Nano*, **19**, 27116-27158. https://doi.org/10.1021/acsnano.5c04200

[15] Price, S. (2024) Reading a Time Temperature Transformation Curve for Metallurgy. https://insights.globalspec.com/article/22799/reading-a-time-temperature-transformation-curve-for-metallurgy

[16] Onike, F., Martin, G.D. and Dunham, A.C. (1986) Time—Temperature—Transformation Curves for Kaolinite. *Materials Science Forum*, **7**, 73-82. https://doi.org/10.4028/www.scientific.net/msf.7.73

[17] Liu, K., Thomas, G., Caballero, A., Moya, J.S. and de Aza, S. (1994) Time-Temperature-transformation Curves for Kaolinite-α-alumina. *Journal of the American Ceramic Society*, **77**, 1545-1552. https://doi.org/10.1111/j.1151-2916.1994.tb09755.x

[18] Long, Z., Xie, G., Wei, H., Su, X., Peng, J., Zhang, P., *et al.* (2009) On the New Criterion to Assess the Glass-Forming Ability of Metallic Alloys. *Materials Science and Engineering*: *A*, **509**, 23-30. https://doi.org/10.1016/j.msea.2009.01.063

[19] Martín, M.I., López, F.A., Alguacil, F.J. and Romero, M. (2014) Development of Crystalline Phases in Sintered Glass-Ceramics from Residual E-Glass Fibres. *Ceramics International*, **40**, 2769-2776. https://doi.org/10.1016/j.ceramint.2013.10.040

[20] Liu, K.C. (1990) Mullite Formation by Reaction Sintering of Kaolinite-Alumina. Ph.D. Thesis, University of California. https://books.google.com.tw/books/about/Mullite_Formation_by_Reaction_Sintering.html?id=l2lLAQAAMAAJ&redir_esc=y

[21] Shang, W., Peng, Z., Huang, Y., Gu, F., Zhang, J., Tang, H., *et al.* (2021) Production of Glass-Ceramics from Metallurgical Slags. *Journal of Cleaner Production*, **317**, Article ID: 128220. https://doi.org/10.1016/j.jclepro.2021.128220

[22] Du, Y., Guo, Y., Wang, G., Zhang, H., Deng, L., Chen, H., *et al.* (2023) Preparation of Glass-Ceramics from Blast Furnace Slag and Its Heavy Metal Curing Properties. *Journal of Material Cycles and Waste Management*, **25**, 3081-3092. https://doi.org/10.1007/s10163-023-01744-2